Progress In Electromagnetics Research, Vol. 126, 1–16, 2012

EFFECT OF REALISTIC MODELING OF DEEP BRAIN STIMULATION ON THE PREDICTION OF VOLUME OF ACTIVATED TISSUE

L. Golestanirad [1, *], A. P. Izquierdo [2], S. J. Graham [1], J. R. Mosig [2], and C. Pollo [3]

[1]Department of Medical Biophysics, University of Toronto, Toronto, Canada

[2]Laboratory of Electromagnetics and Acoustics, Ecole Polytechnique Fédérale de Lausanne (EPFL), Lausanne 1015, Switzerland

[3]Neurosurgery Department, Centre Hospitalier Universitaire Vaudois (CHUV), Lausanne 1011, Switzerland

Abstract—Deep brain stimulation (DBS) is a well-established treatment for Parkinson's disease, essential tremor and dystonia. It has also been successfully applied to treat various other neurological and psychiatric conditions including depression and obsessive-compulsive disorder. Numerous computational models, mostly based on the Finite Element Method (FEM) approach have been suggested to investigate the biophysical mechanisms of electromagnetic wave-tissue interaction during DBS. These models, although emphasizing the importance of various electrical and geometrical parameters, mostly have used simplified geometries over a tightly restricted tissue volume in the case of monopolar stimulation. In the present work we show that topological arrangements and geometrical properties of the model have a significant effect on the distribution of voltages in the concerned tissues. The results support reconsidering the current approach for modeling monopolar DBS which uses a restricted cubic area extended a few centimeters around the active electrode to predict the volume of activated tissue. We propose a new technique called *multi-resolution* FEM modeling, which may improve the accuracy of the prediction of volume of activated tissue and yet be computationally tractable on personal computers.

Received 31 January 2012, Accepted 2 March 2012, Scheduled 8 March 2012

* Corresponding author: Laleh Golestanirad (golestan@sri.utoronto.ca).

1. INTRODUCTION

Deep brain stimulation (DBS) is a well-established highly-effective treatment for Parkinson's disease, (especially in end-stage drug-resistant patients), essential tremor and dystonia [1, 2]. It has also been successfully used to treat various other neurological and psychiatric conditions including depression and obsessive-compulsive disorder [3]. The technique involves delivering electric pulses to the subthalamic nucleus (STN) tissue via an implanted electrode connected to an implanted pulse generator (IPG).

Despite the general effectiveness of DBS, its clinical applications have preceded scientific understanding of its mechanism(s) [4]. The general therapeutic stimulation parameters for DBS (stimulus amplitude, stimulus pulse duration and frequency) have been derived primarily by trial and error [5]. This trial-and-error approach has been effective because of the nearly immediate effects of DBS on the control of tremor and Parkinsonian motor symptoms. However, new therapies utilizing DBS technology will not allow this very simple approach. The beneficial effects of stimulation can take weeks to months to manifest in dystonia and obsessive-compulsive disorder, and it is unclear what electrode geometries, stimulation amplitudes, pulse durations, and frequencies are most effective for these new therapeutic directions [6]. Therefore, future advances in DBS technology are dependent on addressing fundamental questions on its therapeutic mechanism(s) of action. This work is well-suited initially to an electromagnetic modeling approach, given the logistical difficulty of performing exploratory experiments in human and animal subjects.

In bipolar stimulation, as the electric loop goes from one active contact to the other, the IPG influence can be neglected and the assumption seems fully justified. However, in the case of monopolar stimulation, most often used in clinical practice, this assumption is questionable as the electric loop does indeed traverse from the electrode contact to the IPG located in the superior chest. In this case, all the tissues encountered by the electrical current have an impact on the total impedance, and consequently on the current and charges released by the stimulation. However, the authors are not aware of any published work addressing the importance and necessity of considering further tissue compartments in modeling monopolar DBS.

In this work we have extended our previous effort [7] to emphasize the importance of topological arrangements and geometrical properties of the model on the distribution of voltages in the concerned tissues. We used a semi-realistic model based on canonical shapes and showed that changes in the dimensions and positions of those parts of the

body which directly contribute in forming the current path from IPG to the contact electrode may considerably affect the indicators used to predict the volume of activation. We also have studied the effect of uncertainties in the actual values of tissue conductivities on the accuracy of predicted activation volume. To minimize the effect of non-realistic topologies, we have developed a more realistic model of the head and superior chest based on the anatomical data from the Visible Human Project [8]. The study supports our hypothesis that electrical properties of tissues which are directly encountered by the current loop have a non-negligible effect on the distribution of potentials in the vicinity of contact electrodes. Collectively this suggests that to obtain a *quantitatively reliable* estimate of the activation volume for monopolar DBS scheme, it is essential to move on from simplified biological models to more complex models that include anatomically faithful representations and accurate values of electrical properties of concerned tissues.

2. METHODS AND MATERIALS

In the clinical treatment of Parkinson's disease, DBS stimulation is applied with a frequency range of 130–180 Hz and a pulse width of 60–120 µs. In this work we assumed that for the frequency range of clinical DBS, the bioelectromagnetic problem governing the distribution of fields inside the tissue can be considered as quasi-static [9, 10]. Under the quasi-static assumption the scalar potential Φ can be calculated by solving the Laplace equation:

$$\nabla \cdot \sigma \nabla \Phi = 0 \tag{1}$$

where ∇ is the standard differential operator, and σ is the general tensorial conductivity of the biological medium. Once the distribution of potentials is obtained throughout the medium, electric fields and induced currents can be conveniently calculated as $\vec{E} = -\nabla\Phi$ and $\vec{J} = \sigma\vec{E}$, respectively. In this study however, we used the computed electric potential distribution to predict the percentage of activated neurons for different simulation scenarios. A previous study [11] has shown that the activation of a neuron by an extracellular stimulation is directly linked to the double spatial derivative of the external potential along the fiber direction.

We applied the Finite Element Method (FEM) to solve Equation (1) for two biophysical models of interest. The related settings of the FEM solver are explained in the following sections.

2.1. FEM Solver

Both models — a semi-realistic model with canonical shapes, and an anatomically faithful model — were meshed and solved using Ansoft Maxwell3D [12] for approximately 132000 and 634000 tetrahedra, respectively. The Ansoft FEM solver was set to follow an adaptive iterative process whereby an initial mesh was seeded according to the geometrical details of the structure. The scalar potential field Φ was calculated (see Equation (1)) as well as the electric field according to $\vec{E} = -\nabla\Phi$. In our simulations, we set the adaptive solver to refine the mesh for 30% at each iteration and to continue refinement until the difference between two iterative solutions was $< 1\%$.

2.2. Model Development

2.2.1. Electrode and IPG

The model of electrode contacts was based on the DBS electrode manufactured by Medtronic (ACTIVA 3387-Medtronic, Minneapolis, MN, USA). It consists of four cylindrical contacts, each with the diameter of 1.27 mm and length of 1.5 mm, separated by 1.5 mm isolating material (see Figure 1(a)). The tip of the electrode was rounded as to better mimic the manufactured device. We modeled the IPG to resemble the realistic shape of the Medtronic pacemaker (SOLETRA 7426-Medtronic, Minneapolis, MN, USA). In all the simulations, only the upper face of the IPG (which is in direct contact

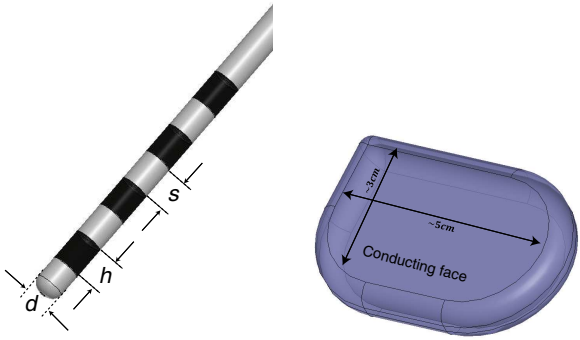

Figure 1. Realistic model of (a) the implanted electrode (ACTIVA 3387) with $h = 1.5$ mm, $s = 1.5$ mm and $d = 1.27$ mm, and (b) the IPG (SOLETRA 7426).

with the skin) was set to be conductive. In accordance with the clinical standards, a fixed voltage of $-2\,\mathrm{V}$ was set on the most distal contact (the lowest cylinder in Figure 1(a)) while the conductor face of IPG was set to $0\,\mathrm{V}$.

2.2.2. Head and Superior Chest Model: Canonical Shapes

To assess the sensitivity of the potential distributions to the geometrical parameters of the model, we first used a simplified canonical shape representation of the head and upper chest (see Figure 2), similar to our previous work [7]. The head and the chest were modeled as parallelepipeds and the spine was modeled by two concentric cylinders (spinal cord surrounded by bone). The gray and white matter were separated into two hemispheres surrounded by cerebrospinal fluid (CSF) and the skull. The rest of the model was composed of muscle, except for including a thin layer of encapsulation tissue surrounding the electrode, which usually forms after implantation and was not included in our previous model. In the acute stage after the implementation, a peri-electrode space is created by the mechanical force of implantation and is filled by extracellular fluid. The effect of changes in this peri-electrode space on the electric field distribution is also reported in some interesting theoretical studies [13, 14]. The profile of current density for both monopolar and pipolar stimulations is given in Figure 3.

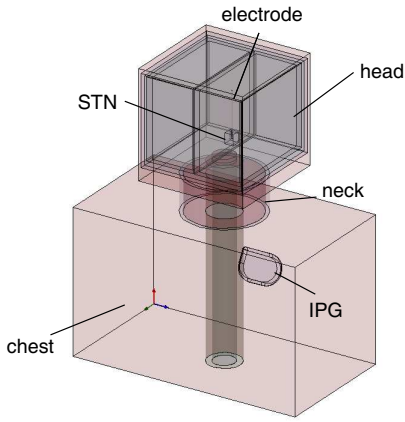

Figure 2. Three-dimensional simplified view of the head, neck and chest with the implanted DBS (electrode and IPG).

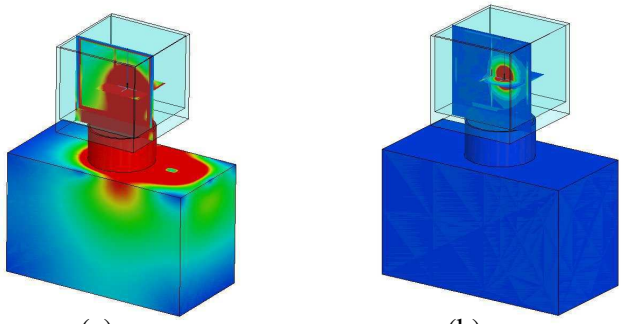

Figure 3. Current density profile in (a) monopolar stimulation with current flowing from active electrode in STN to the IPG in chest, (b) bipolar stimulation with current flowing from one active electrode to the adjacent active electrode in STN.

2.2.3. Head and Superior Chest Model: Anatomical Data

As will be demonstrated in the Section 2.4.1, the distribution of voltages in the vicinity of the electrode in monopolar DBS highly depends on the geometrical features of the whole model. To minimize the effect of non-realistic topologies and focus on the effect of electrical properties of tissues, we built a realistic 3D anatomical model of head and upper chest with the help of Amira, a 3D visualization and volume modeling system [15], that constructs 3D objects from their 2D cross-sectional slices. Three-hundred (300) cross sections of the Visible Human Male data were used with the in-plane resolution of 2048×1216 pixel ($0.3 \times 0.3\,\text{mm}^2$) and the through-plane resolution of 1 mm. The procedure of building the 3D model is similar to the one described in [16].

The final model (Figure 4) consisted of encapsulation tissue (modeled as a layer covering the electrode), white matter and gray matter, CSF and a simplified model of the skull and spinal cord (fine details omitted). These parts were surrounded by bulk muscle covered by a 3 mm layer of skin. To enhance the realism, a thin layer of fat was also modelled surrounding the IPG with the upper face directly contacting the skin. The average thickness of human skin is between 1–5 mm. 3 mm has been chosen as a mean value. However, it has been shown that the model is actually very sensitive to the skin thickness suggesting the need for more patient-specific inquiries. The fat layer around the IPG was 3 mm based on clinical observations.

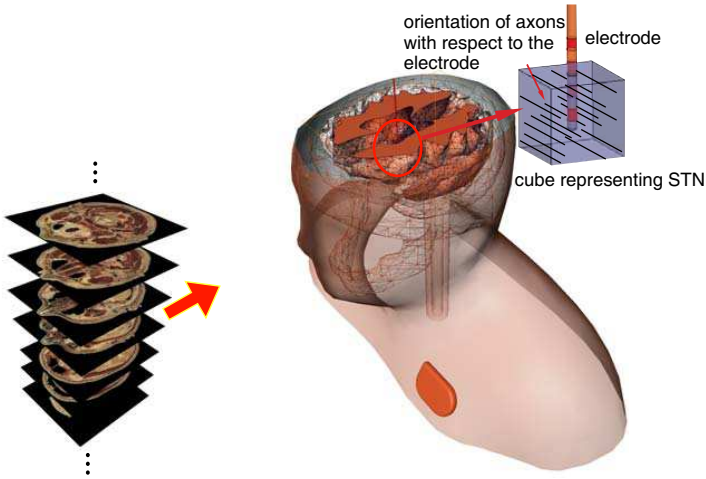

Figure 4. 3D realistic model of head and superior chest. (a) 300 slices from Visible Human Male data set have been used with in-plane resolution of $(0.3 \times 0.3\,\mathrm{mm}^2)$ and through-plane resolution of 1 mm to build 3D objects corresponding to major compartments in the head and chest. (b) A view of the realistic 3D resultant FE model.

After implementing this model in Amira, the number of triangular faces representing a 3D surface created by the surface generator module was far too large for subsequent operations. Thus, the number of triangles was reduced using the surface simplification module. To obtain an object that was compatible with Ansoft 3D modeler, the 3D surface exported from Amira was required to meet certain qualifications. This was assured by applying the Amira *manifold test*. The fact that the final 3D object was required to be manifold imposed some limitations on the degree of surface simplification, especially for objects containing small interior holes. Manual adjustments were necessary in such cases at the level of tissue segmentation.

2.3. Neural Activation Prediction

The NEURON environment tool [17] was used to model axons as already done by others [18, 19]. Here we assumed 5.7 µm-diameter myelinated axons made of 21 nodes of Ranvier separated by 20 internodes. The potential distribution V_0 was extracted from the FEM model of the cubic area representing the STN in the realistic model and applied as the extracellular potential to the electrical model of axons for

the relative orientation of axons and the electrode). The axon response to stimulation was computed for a population of 990 axons distributed uniformly in this cubic area oriented perpendicular to the electrodes axis (Figure 4). The percentage of axons activated was computed for each simulation scenario. A time varying field potential was created by convoluting the obtained potentials by a normalized time varying electric pulse of 60 μs width as is typically used with monopolar DBS.

2.4. Sensitivity Analysis

To quantify the impact of topological and electrical characteristics of the model on the distribution of potentials, the global resistance (R_{Tissue}) was calculated of the tissues encountered by the current released during stimulation. It is important to note that not only the electrical properties of each tissue, but also the shape and overall arrangement of tissues with respect to each other play a role in the overall R_{Tissue} value. For homogeneous tissue, the resistance $R\,[\Omega]$ is given by $R = l/(\sigma A)$ where l [m] is the length of the bulk of tissue, A [m^2] represents its cross-section and σ [S] is its conductivity. In inhomogeneous tissue having different cross-sections however, pertinent to the work under study, resistance is more effectively computed as $R_{\text{Tissue}} = \Delta V/I$ where ΔV is the potential difference between the two electrodes involved in the stimulation. The total current I is computed by the surface integration of the current density on one of the electrode surfaces. R_{Tissue} is an excellent global indicator, as it takes into account any variation of macroscopic conductivity for any tissue.

2.4.1. Effect of Model Geometry

As mentioned in the introduction, in the monopolar DBS scheme, the current loop passes through several major compartments in the head and the superior chest. Our hypothesis is not only that the characteristic conductivities (σ) of tissues which are transversed by the current loop play a decisive role in quantifying the potential distributions, but that the topological features of the model affect the predicted results. To test this hypothesis we altered some of the geometrical parameters of the canonical model depicted in Figure 2 and observed the effect of these changes on the global resistance (R_{Tissue}).

2.4.2. Influence of Tissue Conductivity

The influence of the electrical tissue properties on the potential distribution in electroencephalography (EEG) models has been

investigated in several studies [20, 21], and it has been highlighted that the values of conductivity used for the tissues surrounding the source have an important impact on the potential amplitude and distribution. An interesting literature review on the values of resistivity of different tissues can be found in [21] who evaluated the sensitivity of the forward model of EEG with respect to the resistivity of different classes of tissues. Each class of tissue was set to a mean conductivity value with an upper and lower bound (usually set to $\mp 50\%$ of the mean). Only in the case of widely varying values were other bounds chosen. The range of the chosen lower and upper bounds represented well the resistivity values reported in the literature.

In the present work, the methodology just described was applied to evaluate the model sensitivity to tissue conductivity. The anatomic model (described in Section 2.2.3) was used for this evaluation, as it gives a much more realistic representation of tissue topological arrangements. To evaluate the sensitivity of the model to a specific class of tissue, the conductivity value was set to the upper and lower value, as defined in Table 1, while keeping the other tissue values fixed at the mean value.

3. RESULTS

The effect of geometrical arrangements on the global resistance of the monopolar DBS system is given in Table 2. Of the parameters

Table 1. Human tissue types, isotropic conductivity in S/m and chosen lower and upper bound used in the FEM model.

Tissue	Mean Value [S/m]	Lower Bound [S/m]	Upper Bound [S/m]
Encapsulating tissue	0.10	0.05	0.20
STN	0.23	0.12	0.46
Gray matter	0.10	0.05	0.20
White matter	0.06	0.03	0.12
CSF	2.00	1.00	4.00
Skull	0.08	0.04	0.16
Bone	0.00	0.04	0.16
Spinal cord	0.03	0.01	0.06
Muscle	0.32	0.16	0.64
Skin	0.21	0.11	0.42
Fat	0.02	0.01	0.04

Table 2. Changes in the global resistance, R_{Tissue}, due to changes in the geometrical features of the model.

Parameter	Range (mm)	Change in R_{Tissue} [%]
Width of neck	25–75	−21
Height of neck	25–75	+5
Thickness of skin	1.5–3	−8
Thickness of encapsulation tissue	0.1–1	+27

varied, it can be observed that altering the cross-section of tissues transversed by the current (neck in this example) has a substantial effect on the global resistance of the DBS system and consequently, on the total current driven to the system during the treatment. The thickness of the encapsulation tissue surrounding the electrode is also observed to have a strong influence in accordance with previous reports [19]. It is interesting to note that increasing the thickness of the encapsulation tissue from 0.1 to 1 mm (usual values reported in literature) can increase the global resistance of DBS system up to 27% and a proportional decrease in the transmitted current.

We also investigated the changes in R_{Tissue} caused by the presence of other body organs located inferior to the IPG, (such as heart and lungs) however, the results showed negligible effects ($< 1\%$ change in R_{Tissue}). In other words, an accurate estimation of the voltage distribution around the electrode can be achieved using an accurate anatomical model from IPG up to the electrodes in the STN.

The influence of tissue conductivity on R_{Tissue} and the percentage of neurons activated are summarized in Table 3 using the anatomical model which gives a more accurate account of topological arrangements. Table 3 highlights the importance of tissues which are directly encountered by the current loop. Conductivity of the encapsulating tissue, which is in direct contact with the stimulating electrode, plays an important role in determining the percentage of activated neurons in the STN. Choosing the lower conductivity value for this layer results in a higher voltage drop over it, decreasesing the voltage drop over the STN. This effect in turn decreases the number of activated neurons in the STN, as the neural activation function is proportional to the second derivative of the voltage.

The electrical parameters of the STN have also a determining effect on the volume of activated tissue. However, the trend is quite different than for the encapsulating tissue. For STN, increasing the conductivity was observed to decrease the number of activated neurons. Again, the activation function of neurons exposed to an external

Table 3. Sensitivity of the model of monopolar DBS to the tissue conductivities.

	R_{Tissue} [Ω]		Change in R_{Tissue} [%]		Neurons Activated [%]	
Type of Tissue	σ_{upper}	σ_{lower}	σ_{upper}	σ_{lower}	σ_{upper}	σ_{lower}
Encapsulating tissue	803.21	1470.59	-22.49	$+41.91$	12.6	1.7
STN	888.89	1315.79	-14.22	$+26.97$	0.0	17.4
Grey Matter	990.10	1117.32	-4.46	$+7.82$	8.2	5.2
White Matter	1015.23	1058.20	-2.03	$+2.12$	7.0	7.0
CSF	1036.27	1041.67	-0.0	0.52	7.0	7.0
Skull	1036.27	1041.67	-0.0	$+0.52$	7.0	7.0
Spinal cord	1036.27	1036.27	-0.0	$+0.0$	7.0	7.0
Bone	1036.27	1036.27	-0.0	$+0.0$	7.0	7.0
Muscle	1005.03	1086.96	-3.02	$+4.89$	7.2	6.1
Skin	1000.00	1081.08	-3.50	$+4.32$	7.5	6.2
Fat	1005.03	1086.96	-3.02	$+4.89$	7.2	6.1
base model	1036.27		0		7.0	

voltage distribution is proportional to the second derivative of the voltage along the neuron axis. When the conductivity of the STN region is increased, the voltage drop over the region becomes smaller and consequently the second derivatives of this voltage take smaller values. This translates to a smaller activation function in the area leading to decreased neuronal activation.

4. DISCUSSION AND CONCLUSION

The mechanism(s) of action underlying DBS of STN are still under evaluation as the structures influenced by the DBS are matter of debate. In fact, it has been suggested that not only the STN neurons themselves, but also the activation of axons surrounding the STN may contribute in the improvement of disease symptoms [4]. It is obvious however, that a meaningful interpretation of clinical observations would not be possible without an accurate estimation of the volume of tissue activated (VTA). Currently, the standard approach adopted by almost all the active research groups in the field, is based on applying 3D FEM on a restricted cubic area extended a few centimeters around the active electrode. On the other hand, extensive computational effort is usually undertaken to accurately model the anatomical geometry

of nearby organs using MRI of patients, or to account for electrical anisotropies using DTI data.

In this study we highlighted the effect of further tissue compartments on the indicators conventionally used to predict the VTA in monopolar DBS modeling. The canonical model described in Section 2.2.2, although providing a very simplified representation of the DBS system, was still able to demonstrate clearly the importance of geometrical features of the model on the prediction of activated area. Table 2 gives four examples of changes in geometrical parameters of the model which significantly change the impedance of tissues between the active contact and the IPG, and consequently, the magnitude of electric currents sent to designated areas. Although the mean value of the impedance obtained using the computational model was approximately 1 kΩ, in accordance with the measurements performed in patients having implanted systems [22], the variations observed due to geometrical features suggest that for an accurate estimation of volume of activated tissues, an anatomically realistic representation of the system which includes further compartments in the neck and the upper chest is required. In other words, it is shown that the result of VTA prediction is highly sensitive to the geometrical representation and electrical properties of the model, suggesting that more research is needed to be performed in this area.

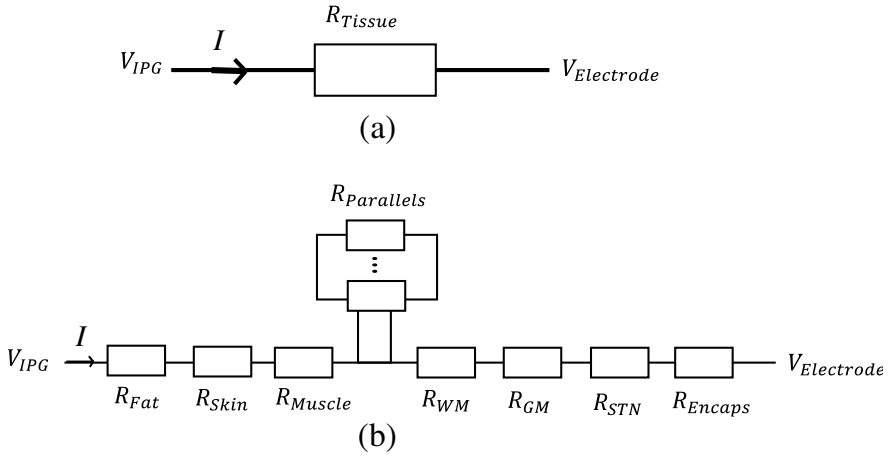

Figure 5. The global resistance of tissues between the IPG and the contact electrode in monopolar DBS scheme, (a) the equivalent resistance, (b) two categories of tissues encountered by current through its path from the IPG to contact electrode.

4.1. Towards Intelligent Model Development

As rule of thumb, to assess the effect of different tissues on the voltage distribution around the active electrode, we can classify tissues in two categories depending on whether current is *required* to pass through them on the path from the IPG to the stimulating electrode, or the current *can partially* pass through them. Considering that the IPG is always implanted with its conductor side in contact with the skin, the former category includes: skin, fat (in the vicinity of the conductive face of the IPG), pectoral muscles, brain tissues (white and gray matter), targeted zones in the brain (usually STN, GPi or Vim) and the layer of encapsulating tissue formed around the stimulating electrode after surgery. Other organs and tissues through which current can partially pass are CSF, other brain structures such as the brain stem,

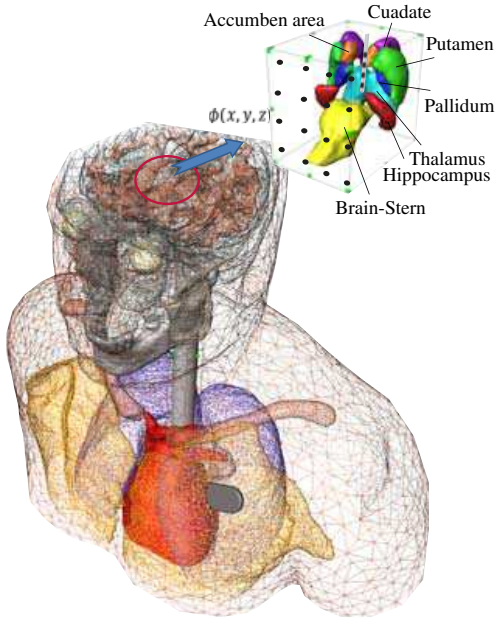

Figure 6. Multi-resolution model of monopolar DBS. (a) A large-scale low resolution (1 cm) model of head, neck and upper chest. The voltage distribution can be computed throughout the model, (b) the voltage distribution has been exported to a high-resolution ($<$ 1 mm) FEM model containing the detailed anatomical representation of subcortical tissues. As the second model covers a small area surrounding the electrode, the total number of unknowns would be in the range which can be handled on a typical PC.

the esophagus, vessels, the trachea, and the spinal cord. Figure 5 shows a lumped-parameter circuit model of the current path from the IPG to the electrode in the monopolar DBS scheme, according to these categories. It can be observed from Table 3 that tissues in the vicinity of the IPG or the electrode have more effect on the global indicators of neuronal activation. This information can be used as part of building accurate and yet efficient models of monopolar DBS which rigorously model effective tissues and ignore fine details of further components.

One possible approach that stems from this realization is the development of *multi-resolution* FEM models. In the conventional approach of modeling monopolar DBS, the outer boundary of the cubic computational area is grounded (set to zero volts). The accuracy of the model can be improved by computing a more realistic voltage distribution on the surface of this boundary using a large-scale relatively low-resolution (e.g., 1 cm mesh size) model of head, neck and upper chest (see Figure 6). In this approach, we first build an FEM model which contains influential tissue compartments in the head, neck and upper chest to compute the potential distribution $\Phi(x, y, z)$ on the boundary of an imaginary cube centered at the active electrode. However as this model does not include very fine details of subcortical tissues in the vicinity of the active electrode, the overall computational burden would be reasonably moderated. In the next step, the computed potential distribution can be fed to second high-resolution FEM model which contains the detailed geometrical representation of subcortical tissues in the vicinity of the active electrode. This technique has potential to improve the accuracy of the predicted VTA in monopolar DBS scheme. It can also serve as a basis for more efficient analysis of safety aspects of DBS [23]. Application and verification of this technique will be the subject of future work.

ACKNOWLEDGMENT

This work was supported by research grants from Swiss National Science Foundation (grant number 31-108318 and PBELP2-135868).

REFERENCES

1. Rodriguez-Oroz, M. C., J. A. Obeso, A. E. Lang, J.-L. Houeto, P. Pollak, S. Rehncrona, J. Kulisevsky, A. Albanese, J. Volkmann, M. I. Hariz, N. P. Quinn, J. D. Speelman, J. Guridi, I. Zamarbide, A. Gironell, J. Molet, B. Pascual-Sedano, B. Pidoux, A. M. Bonnet, Y. Agid, J. Xie, A.-L. Benabid, A. M. Lozano,

J. Saint-Cyr, L. Romito, M. F. Contarino, M. Scerrati, V. Fraix, and N. V. Blercom, "Bilateral deep brain stimulation in Parkinson's disease: A multicentre study with 4 years follow-up," *Brain*, Vol. 128, No. 10, 2240–2249, Oct. 2005. [Online]. Available: http://dx.doi.org/10.1093/brain/awh571.

2. Wider, C., C. Pollo, J. Bloch, P. R. Burkhard, and F. J. Vingerhoets, "Long-term outcome of 50 consecutive Parkinson's disease patients treated with subthalamic deep brain stimulation," *Parkinsonism Relat. Disord.*, Vol. 14, No. 2, 114–119, 2008. [Online]. Available: http://dx.doi.org/10.1016/j.parkreldis.2007.06.012.
3. Gabriels, L., P. Cosyns, B. Nuttin, H. Demeulemeester, and J. Gybels, "Deep brain stimulation for treatment-refractory obsessive compulsive disorder: Phsychopathological and neuropsychological outcome in three cases," *Acta Psychiatr. Scand.*, Vol. 107, 275–282, 2003.
4. McIntyre, C. C., M. Savasta, L. Kerkerian-Le Goff, and J. L. Vitek, "Uncovering the mechanism(s) of action of deep brain stimulation: Activation, inhibition, or both," *Clin. Neurophysiol.*, Vol. 115, No. 6, 1239–1248, Jun. 2004. [Online]. Available: http://dx.doi.org/10.1016/j.clinph.2003.12.024.
5. Moro, E., J. A. Esselink, J. Xie, A. L. Benabid, and P. Pollak, "The impact on parkinsons disease of electrical parameter settings in STN stimulation," *Neurology*, Vol. 59, 706–713, 2002.
6. McIntyre, C. C., M. Savasta, B. L. Walter, and J. L. Vitek, "How does deep brain stimulation work? Present understanding and future questions," *J. Clin. Neurophysiol.*, Vol. 21, 40–50, 2004.
7. Walckiers, G., B. Fuchs, J.-P. Thiran, J. R. Mosig, and C. Pollo, "Influence of the implanted pulse generator as reference electrode in finite element model of monopolar deep brain stimulation," *J. Neurosci. Methods*, Vol. 186, No. 1, 90–96, Jan. 2010. [Online]. Available: http://www.ncbi.nlm.nih.gov/pubmed/19895845.
8. EPFL Computer Science Departement, Visible Human Project, [Online]. Available: http://visiblehuman.epfl.ch/.
9. Van den Broek, S. P., H. Zhou, and M. J. Peters, "Computation of neuromagnetic fields using finite-element method and Biot-Savart law," *Med. Biol. Eng. Comput.*, Vol. 34, No. 1, 21–26, 1996.
10. Miller, C. E. and C. S. Henriquez, "Finite element analysis of bioelectric phenomena," *Crit. Rev. Biomed. Eng.*, Vol. 18, No. 3, 207–233, 1990.
11. Rattay, F., "Analysis of models for extracellular fiber stimulation," *IEEE Trans. Biomed. Eng.*, Vol. 36, No. 7, 676–682,

Jul. 1989.

12. ANSYS, Inc., Maxwell 3D, [Online]. Available: http://www.ansoft.com/products/em/maxwell.
13. Yousif, N., R. Bayford, S. Wang, and X. Liu, "Quantifying the effects of the electrode-brain interface on the crossing electric currents in deep brain recording and stimulation," *Neuroscience*, Vol. 152, 68391, 2008.
14. Yousif, N. and X. Liu, "Investigating the depth electrode-brain interface in deep brain stimulation using finite element models with graded complexity in structure and solution," *J. Neurosci. Methods*, Vol. 184, No. 1, 142–151, 2009.
15. Visage Imaging GmbH, Amira 5.2-User's guide and reference manual, [Online]. Available: http://www.amira.com/, 2001.
16. Golestanirad, L., M. Mattes, J. R. Mosig, and C. Pollo, "Effect of model accuracy on the result of computed current densities in the simulation of transcranial magnetic stimulation," *IEEE Transactions on Magnetics*, Vol. 46, No. 12, 4046–4051, 2010.
17. Hines, M. L. and N. T. Carnevale, "Neuron: A tool for neuroscientists," *Neuroscientist*, Vol. 7, No. 2, 123–135, Apr. 2001.
18. Butson, C. R. and C. C. McIntyre, "Tissue and electrode capacitance reduce neural activation volumes during deep brain stimulation," *Clin. Neurophysiol.*, Vol. 116, No. 10, 2490–2500, Oct. 2005. [Online]. Available: http://dx.doi.org/10.1016/j.clinph.2005.06.023.
19. Butson, C. R., C. B. Maks, and C. C. McIntyre, "Sources and effects of electrode impedance during deep brain stimulation," *Clin. Neurophysiol.*, Vol. 117, No. 2, 447–454, 2006.
20. Ramon, C., P. Schimpf, and J. Haueisen, "In uence of head models on eeg simulations and inverse source localizations," *BioMedical Engineering OnLine*, 2006.
21. Haueisen, J., C. Ramon, M. Eiselt, H. Brauer, and H. Nowak, "In uence of tissue resistivities on neuromagnetic fields and electric potentials studied with a finite element model of the head," *IEEE Trans. Biomed. Eng.*, Vol. 44, No. 8, 727–735, Aug. 1997. [Online]. Available: http://www.ncbi.nlm.nih.gov/pubmed/9254986.
22. Volkmann, J., J. Herzog, F. Kopper, and G. Deuschl, "Introduction to the programming of deep brain stimulators," *Mov. Disord.*, Vol. 17, No. 3:S, 181–187, 2002.
23. Mohsin, S. A., N. M. Sheikh, and U. Saeed, "MRI induced heating of deep brain stimulation leads: Effect of the air-tissue interface," *Progress In Electromagnetics Research*, Vol. 83, 81–91, 2008.